The whole behavioral spectrum of jointed rock slopes

Shahrzad Roshankhah[1*^] and Kami Mohammadi[1]

[1] Civil and Environmental Engineering Department, University of Utah, Salt Lake City, UT, USA.

* Corresponding author information: shahrzad.roshankhah@utah.edu, 1-801-585-0358
^ Presenting author

1. Abstract

With the new required analyses for the sustainability and resiliency of infrastructure, there is a need to understand and quantify the whole behavioral spectrum of the geomaterials that make or support the infrastructure. This study aims at understanding the mechanical behavior of jointed rock slopes from pre-failure state to failure and post-failure states. Progressive failure of slopes made up of jointed rocks occurs when the collapse of a critical part causes confinement loss and failure of other parts of the structure. In this study, we use the finite-discrete element method to analyze the failure and post-failure states of several jointed rock slopes with different joint patterns. The mechanical properties of the rock matrix and joints are kept constant for all the models, but the joints' spacing and their orientation relative to the slope angle are varied. The initial failure is triggered in joints and interfacial contact elements by a strength reduction mechanism. The results indicate the failure mechanism and other parameters important for the analyses and design of resilient infrastructure surrounding the slopes. These parameters include, for example, the kinetic energy released by the failed material, as well as the runout volume and the runout distance of the failed materials.

2. Introduction

Understanding the progressive failure of jointed rock slopes is the subject of research for a relatively long time, and it is still relevant (e.g., Goodman & Bray 1977, Dowding et al. 1983, Barton et al. 1985, Duncan 1996, Zuo et al. 2005, Zhang et al. 2015; Zheng et al. 2018, Jiang et al. 2021, and references therein). The reason for the endurance of this challenge is that the failure of this material occurs through complex interactions between the pre-existing natural fracture network and the newly generated tensile and shear fractures in the rock blocks, layers, or columns. As a result, the jointed rock slope may experience many scenarios depending on the material properties and geometric characteristics of the discrete fracture network (DFN). Analytical methods, like limit equilibrium, can only apply to statistically homogenous and isotropic geomaterials, such as slopes made up of soils and very heavily jointed rocks. These methods can only predict one failure plane with the highest probability of failure. Thus, they cannot show the complex stress-strain distributions among the DFNs interacting with the intact blocks and multiple failure planes growing through sliding, rotating, and dividing rock blocks. The post-failure response of the slope, such as the maximum runout volume and distance of the failed materials, are also unknown with these methods.

Appropriate numerical simulations can shed light on the failure patterns in jointed rock slopes (Lisjak & Grasselli 2014). Continuum-based finite element methods would need to use sophisticated functions and some non-physical parameters to implement a limited number of DFNs, with which the nucleation and propagation of the failure plane must be on predefined pathways (Blair & Cook 1998, Ma et al. 2011). Discrete element-based methods can implement DFNs in a more natural way. i.e., as the interface between discrete rock blocks interacting with each other, but the discontinuities that comprise the global failure plane can still be only limited to the interfaces (Cundall & Hart 1992). To capture fractures through the rock blocks, some extensions to DEM methods have been adopting bonded particles to represent the rock blocks, which makes the computations even more expensive (Damjanac et al. 2015). A better computational scheme is one that integrates principles of continuum mechanics with discrete element interaction algorithms and takes advantage of their strengths, i.e., the efficiency of FEM and the more realistic modeling capability of DEM. These are hybrid finite-discrete element methods (FDEM) that can capture the transition of a jointed rock mass, consisting of intact rock blocks and closed pre-existing fractures in the natural state, from an initial semi-continuum state to a semi-discrete state when it is subjected to various hydromechanical perturbations. The next section summarizes the principles of this method. In this study, we investigate the mechanical response of several jointed rock slopes with various DFN characteristics. Specifically, inclined (low angle with respect to the slope angle), and anti-inclined (high angle with respect to the slope angle)

persistent joints crossed by non-persistent joints are modeled with two different spacings for the persistent joints. These two distinct structures are observed in many rocks hosting a variety of civil infrastructure. The shear strength of jointed rocks increases with decreasing the spacing between the joints because lower deformations are needed to mobilize the frictional shear strength between the smaller rock blocks (Barton & Bandis 1982).

3. Computational formulation

In FDEM formulation, the problem domain is first discretized with three-node finite elements, which deform based on the assigned elastic properties (e.g., Young's modulus and Poisson's ratio) but cannot break. Between each pair of finite elements, a four-node crack element is embedded, which can break if the resultant stresses on it exceed the assigned strength properties (tensile strength, friction coefficient, cohesion, and fracture energy). Fig. 1 shows schematic views of the discretized domain and the failure criteria for the crack elements in tension (mode-I) and shear (mode-II).

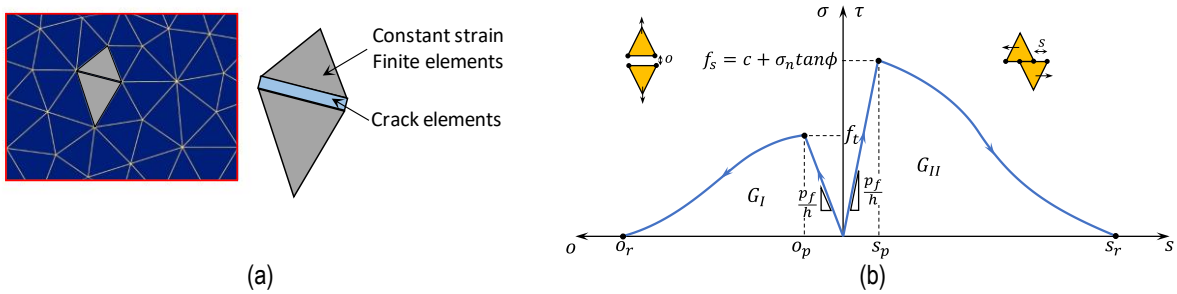

Figure 1. Schematic representation of FDEM formulation. (a) three-node finite elements interfaced by four-node crack elements. (b) Nonlinear fracture mechanics criteria for the response of crack elements in opening and shear failure modes (after Lisjak et al 2017).

An explicit second-order finite difference time integration scheme solves the equation of motion for each node to determine the displacement *u* (m) of the elements with mass *M* (kg) and damping *C* (kg/s) tensors (Geomechanica 2021).

$$M\ddot{u} + C\dot{u} + F_{int}(u) = \bar{F}_{ext}(u)$$

In conventional finite element formulations, the internal forces F_{int} (N) and external forces $\bar{F}_{ext}$ (N) include the forces due to internal elastic deformations F_e (N), external mechanical loads F_{ext} (N), and imposed fluid pressure F_{fl} (N). In FDEM, however, two more components are involved, i.e., the crack element bonding forces F_b (N) and the contact forces F_c (N):

$$F_{int}(u) = F_e(u) + F_b(u)$$

$$\bar{F}_{ext}(u) = F_{ext}(u) + F_{fl}(u) + F_c(u)$$

The bonding force comes from the nonlinear fracture mechanics model for each fracture mode. The bond force is found as a function of crack displacement as shown by *o* (opening) and *s* (shearing) in Fig. 1b. If the displacements of a crack element exceed the corresponding critical displacements o_p and s_p, stresses reach the shear or tensile strength, hence it fails (Munjiza & Andrews 2000). The evolution of crack displacement depends on crack fracture energy. Once a crack element is broken, the separated finite elements are treated as discrete elements, and contact forces are calculated for them. The contact force consists of two components, the repulsive force F_{rep} (N) and the frictional force F_{fri} (N).

$$F_c(u) = F_{rep}(u) + F_{fri}(u)$$

The repulsive force is found from the penalty function method by integrating an infinitesimal repulsive force that is induced due to an infinitesimal overlapping area between the two interacting elements (Munjiza & Andrews 2000).

$$F_{rep}(u) = \sum_{i=1}^{n}\sum_{j=1}^{m}\int_{\beta_t \cap \beta_c}\left[\nabla\phi_{cj}(P_c) - \nabla\phi_{ti}(P_t)\right]dA$$

The contact stiffness is introduced through the normal and tangential penalty functions, and the overlapping area is the common perimeter of the two contacting bodies $\beta t \cap \beta c$. The frictional force F_{fri} is obtained from Coulomb's friction law.

$$F_{fri}(u) = min\left[p_t|s|, \left|\sigma_n tan\varphi_f\right|\right]dA$$

4. Model configurations and material properties

Four two-dimensional models of 15 m high jointed rock slopes with α=45° slope angles are constructed. The jointed rock is blocky with blocks' aspect ratio of *s:d*=1:2 and 50% overlap between them. Two different relative angles between the slope and continuous joints are modeled, i.e., α:γ=3:1 and 1:2.5, which correspond to γ=15° and 115° and are called low-angle (inclined) and high-angle (anti-inclined) models, respectively. Also, two different spacings between the continuous joints are modeled, i.e., the spacings normalized by the slope height are *s:H*=1:3 and 1:15. These are called coarse and fine models respectively. The bottom boundary of the models is fixed in both horizontal and vertical directions and the lateral boundaries are fixed in the horizontal direction. Gravity effects are on, and geostatic stresses equilibrate with an initial FEM simulation of 500,000 time-steps (Δt=2 μs). All models are discretized with about 180,000 triangular finite elements. Fig. 2 shows the geometry and DFN configuration of the four models in this study.

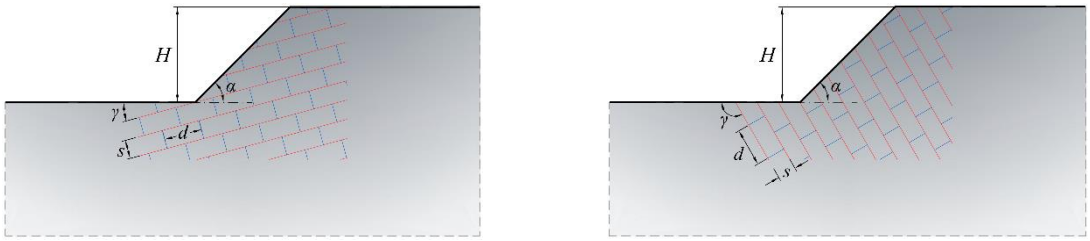

(a) (b)

Figure 2. Geometric configurations for the (a) low-angle models, (b) high-angle models. Fine and coarse blocks are modeled by s:H=1:15 and 1:5, respectively.

Material properties are listed in Table 1. The crack energies in modes I & II and normal & tangential penalties are calibrated during the numerical calibration procedure to match the material's unconfined compressive strength.

Table 1. Material properties used in the numerical simulations.

Properties	**Finite elements**	
Young's Modulus (GPa)	0.59	
Poisson's Ratio	0.29	
Bulk Mass Density (kg/m^3)	2680	
	Crack elements	**Discrete fractures**
Tensile Strength (kPa)	50	10
Friction Angle (°)	30	11
Cohesion (kPa)	100	50
Mode-I Crack Energy (N/m)	130	13
Mode-II Crack Energy (N/m)	1300	130
Normal Fracture Penalty (GPa.m)	5.9	5.9
Tangential Fracture Penalty (GPa/m)	917	917

The failure is triggered by reducing the cohesive and frictional strength of both interfacial crack elements and discrete fractures with a rate of 10% per 10,000 time steps until 30% of the initial strength remains.

5. Results and discussions

Strength reduction of interface crack elements and DFNs results in movement of a portion of the rock mass which involves opening and shearing of DFNs and cracking of intact rock blocks along critical paths. The displacement field of the jointed rock slopes is presented in figure 3. The displacements are shown in two middle and end of failure stages. The activated or broken joints are shown with solid black lines. With small spacings between the persistent joints, a large rock wedge consisting of many rock blocks slides along a critical persistent joint that crosses the slope toe with a low

angle, but flexural toppling failure is observed in the high angle model. Regardless of the failure mechanism, the maximum displacement observed in both models exceeds 20 meters.

Increasing the thickness of rock layers or columns (spacing between the persistent joints) increases the flexural resistance of the rock columns (displacements about 2 cm) and may decrease the size of the unstable wedge. The latter would be the case if the next persistent joint does not cross the slope toe. In this case, the runout volume and distance would be less than the case with small spacing. Note that all cases experiencing global collapse, show the creation of multiple failure planes propagating through pre-existing DFN and intact rock blocks, however, a portion of the failed volume may be kinematically locked and stopped further movement. These features cannot be explored by analytical techniques, like limit equilibrium, pure finite element, or pure discrete element modeling techniques.

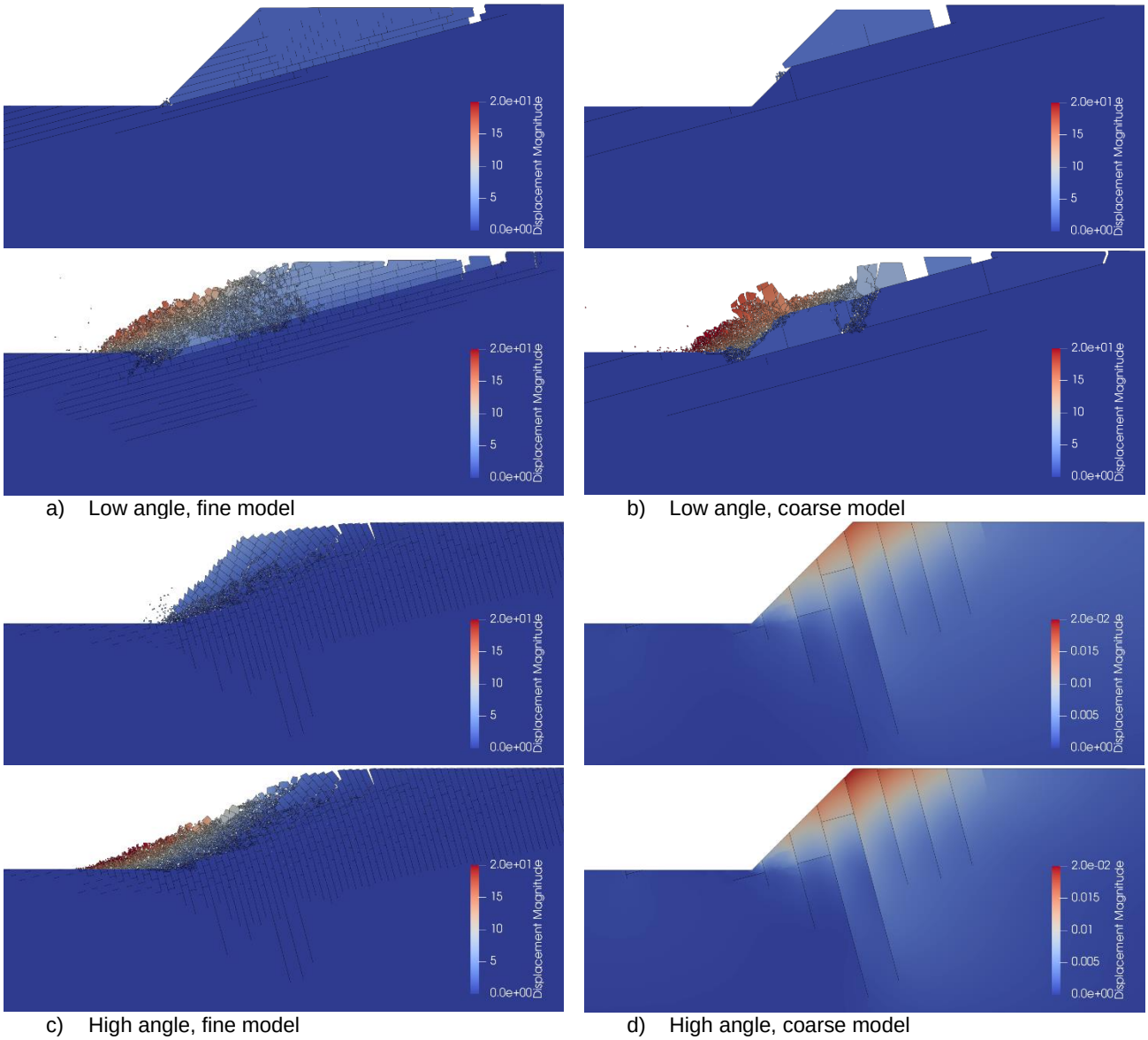

a) Low angle, fine model

b) Low angle, coarse model

c) High angle, fine model

d) High angle, coarse model

Figure 3. progressive failure of jointed rock slopes with different configurations during and after the collapse.

6. Conclusions

The hybrid finite-discrete element modeling of jointed rock slopes provides the opportunity to study the whole spectrum of the slopes' response to perturbations. That is, the transition of the geomaterial from an apparently continuous state (rock with weakly cemented DFNs) to a discrete state is captured. Sliding and flexural toppling failure mechanisms are observed for inclined (low angle) and anti-inclined (high angle) models with small and large spacing between the persistent joints. Regardless of the dominant failure mechanism, lower spacing between the persistent joints provides lower flexural strength for the rock layers and columns, which leads to larger failed volume and longer runout distance.

7. Acknowledgments

The authors acknowledge the funding provided by the Department of Civil and Environmental Engineering at the University of Utah.

8. References

Barton, N, and Bandis, S. 1982. Effects of block size on the shear behavior of jointed rocks. The 23rd U.S Symposium on Rock Mechanics (USRMS), Berkeley, California, August 25, ARMA-82-739.

Barton, N, Bandis, S, and Bakhtar, K. 1985. Strength, deformation and conductivity coupling of rock joints. International Journal of Rock Mechanics and Mining Sciences, Geomechanics Abstracts 22(3),121–140.

Cundall, PA, and Hart, RD. 1992. Numerical modelling of discontinua. Engineering Computations 9(10), 1–13.

Damjanac, B, Detournay, C, Cundall, PA. 2015. Application of particle and lattice codes to simulation of hydraulic fracturing, Computational Particle Mechanics, 1–13.

Dowding, CH, Belytschko, TB, and Yen, HJ. 1983. Dynamic computational analysis of opening in joint rock, Journal of Geotechnical Engineering, ASCE 109, 1551–1556.

Duncan, M. 1996. State of the art: limit equilibrium and finite-element analysis of slopes. Journal of Geotechnical Engineering, ASCE 122(7), 577–596.

Geomechanica Inc. 2021. Irazu Software. Theory Manual. Toronto, Canada.

Goodman, RE, and Bray, JW. 1977. Toppling of rock slopes. Rock Engineering for Foundations & Slopes. ASCE 201–234.

Griffiths, DV, and Lane, PA. 1999. Slope stability analysis by finite elements. Geotechnique 49(3), 387–403.

Jiang, M, Niu, M, Zhang, F, Wang, H, and Liao, Z. 2021. Instability analysis of jointed rock slope subject to rainfall using DEM strength reduction technique, European Journal of Environmental and Civil Engineering, 1–24.

Lisjak, A, Kaifosh, P, He, L, Tatone, BSA, Mahabadi, OK, and Grasselli, G. 2017. A 2D, Fully-coupled, hydromechanical, FDEM formulation for modeling fracturing processes in discontinuous, porous masses. Comp. Geotech. 81, 1–18.

Munjiza, A, and Andrews, KRF. 2000. Penalty function method for combined finite-discrete element systems comprising a large number of separate bodies. Int. J. Numer. Meth. Engng. 49, 1377–1396.

Zhang, K, Cao, P, Meng, J, Li, K, and Fan, W. 2015. Modeling the Progressive Failure of Jointed Rock Slope Using Fracture Mechanics and the Strength Reduction Method, Rock Mechanics and Rock Engineering 48, 771–785.

Zheng, Y, Chen, C, Liu, T, Zhang, H, Xia, K, and Liu, F. 2018. Study on the mechanisms of flexural toppling failure in anti-inclined rock slopes using numerical and limit equilibrium models, Engineering Geology 237, 116–128.

Zuo, BC, Chen, CX, Lie, XW, and Shen, Q. 2005. Modeling experiment study on failure mechanism of counter-tilt rock slope. Chin. J. Rock Mech. Eng. 34, 3505–3511.